The 2014 World Congress on
Advances in Civil, Environmental, and Materials Research (ACEM14)
Busan, Korea, August 24-28, 2014

Flutter performance of central-slotted plate under large wind attack angles

* Hao-jun Tang [1)] and Yong-le Li [2)]
[1), 2)] *Department of Bridge Engineering, Southwest Jiaotong University, Chengdu 610031, China*
[1)] *tanghj1201@163.com*

ABSTRACT

Aerodynamic stability is one of the most important themes in the design of long-span bridges. The plate and the central-slotted plate are chosen as objects of study, using ANSYS software and CFD software FLUENT to analyze their flutter performance. Based on theoretical flutter derivatives of thin plate, the effect of constant term on calculation result is firstly analyzed. The aerodynamic coefficients and flutter derivatives of plate are further calculated and compared with theoretical solution. Moreover, the effects on the flutter performance of central-slotted plate are discussed under the condition of various slot widths and wind attack angles after checking the reliability of the analysis method. Results show that wind attack angle and slot width have significant influence on the flutter performance of plate. The flutter critical wind speed decreases with the increase of wind attack angle, and it increases with the increase of slot width when the value of wind attack angle is 0 or 2 degrees.

1. INTRODUCTION

In the recent years the long process leading to an appropriate bridge design has become more complex. Aerodynamic stability is one of the most important themes in the design of long-span bridges. The design of long-span bridges has urged special attention to the prevention of flutter occurrence. Current theories for analyzing the responses of bridges to wind are based on their flutter derivatives, which can be extracted from wind tunnel test or numerical simulation. Many methods for analyzing the flutter problem of long-span bridges have been developed. These methods are usually solved in the frequency domain and can be divided into two types. One type is based on the natural modal coordinates of structure and the linear superposition principle, so it is called the multimode flutter analysis. (Scanlan 1978) established a basic theory for the multimode flutter analysis of long-span bridges and also suggested a mode-by-mode approach. (Namini 1992) proposed the pK-F method for multimode flutter analysis based on p-K method which was widely used in aviation field. This method was determining the preflutter and postflutter responses by solution to the modal equations of motion. (Chen 1994) transferred the flutter problem into a Mth-order complex-number generalized eigenvalue problem and proposed the M-S method. (Ding 2002) proposed a multimode flutter analysis of long-span bridges based on Scanlan's linear self-excited forces which was single-parameter, non-iterative and offers simplicity, automaticity and robustness. The other type for flutter prediction is based on

[1)] Doctoral Candidate
[2)] Professor

the full-order physical model of bridge structures. (Miyata 1990) first presented a direct flutter analysis, in which the iterative search process was not required but the computational complexity was still very large. (Ge 2000) also proposed a 3D-flutter analysis of long-span bridges by the full-mode approach with high calculation efficiency, in which the effect of structural damping was considered effectively. (Hua 2007) proposed a finite element model and frequency analysis method for analyzing 3-D full-order flutter of long-span bridges using ANSYS software. This method utilized a special kind of element Matrix27 in ANSYS to simulate the aeroelastic forces acting on bridges.

Aerodynamic method is usually an effective countermeasure for flutter suppression, by increasing the flutter critical wind speed of a bridge. Good aerodynamic performance of a bridge deck can be achieved by using shallow sections, closed sections, streamline edges and other minor and more subtle changes to the cross-sectional geometry. (Steinman 1956) described the Mackinac Bridge had complete and absolute aerodynamic stability against all forms of oscillation in all modes, at all wind velocities and all angles of attack. The high aerodynamic stability was the provision of wide open spaces between the stiffening trusses and the outer edges of the roadway. (Miyata 1993) described some design considerations of wind effects of the Akashi Kaikyo Bridge to find aerodynamic means for reducing the flutter instability. This resulted in a median barrier installed at the center of the deck floor, which remarkably raised the critical wind speed. (Sato 2002) confirmed that slotted box girder was applicable for the super long-span bridge by full aeroelastic model test. However, there is no unified understanding how to choose reasonable aerodynamic methods, and the influence mechanism of aerodynamic method is not clear.

In this paper, the plate and the central-slotted plate are chosen as objects of study, using ANSYS software and CFD software FLUENT to analyze their flutter performance. Based on theoretical flutter derivatives of thin plate, the effect of constant term on calculation result is firstly analyzed. The aerodynamic coefficients and flutter derivatives of plate are further calculated and compared with theoretical solution. Moreover, the effects on the flutter performance of central-slotted plate are discussed under the condition of various slot widths and wind attack angles after checking the reliability of the analysis method.

2. ANALYSIS METHOD FOR FLUTTER

2.1 Basic theory of ANSYS method

Due to the lack of available modules, ANSYS cannot be directly used for flutter analysis. (Hua 2007) proposed a method for analyzing flutter using ANSYS software. The dynamic equations of a bridge surrounded by the smooth flow as shown in Eq. (1)

$$\mathbf{M}\ddot{\mathbf{X}} + \mathbf{C}\dot{\mathbf{X}} + \mathbf{K}\mathbf{X} = \mathbf{F}_{ae} \tag{1}$$

where $\mathbf{M}$, $\mathbf{C}$, and $\mathbf{K}$ are the structural mass, damping, stiffness matrices, respectively, $\mathbf{X}$, $\dot{\mathbf{X}}$, $\ddot{\mathbf{X}}$ the nodal displacement, velocity and acceleration vectors, respectively. $\mathbf{F}_{ae}$ is the vector of the equivalent nodal aeroelastic forces. The self-excited forces per unit span (Scanlan 1993) as shown in Eq. (2)

$$L_{\text{ae}} = \frac{1}{2}\rho U^2(2B)\left\{KH_1^*\frac{\dot{h}}{U} + KH_2^*\frac{\dot{\alpha}B}{U} + K^2H_3^*\alpha + K^2H_4^*\frac{h}{B}\right\} \tag{2a}$$

$$M_{\text{ae}} = \frac{1}{2}\rho U^2(2B^2)\left\{KA_1^*\frac{\dot{h}}{U} + KA_2^*\frac{\dot{\alpha}B}{U} + K^2A_3^*\alpha + K^2A_4^*\frac{h}{B}\right\} \tag{2b}$$

where ρ is the air density, U the mean wind velocity, B the bridge deck width, $K = \omega B/U$ the reduced frequency, ω the circular frequency of vibration, h, and α are the vertical, and torsional displacements, respectively, $\dot{h}$, and $\dot{\alpha}$ are the vertical, and torsional velocities, respectively, and H_i^*, A_i^* (i=1-4) the non-dimensional flutter derivatives. Converting the distributed self-excited forces on bridge deck element e into equivalent nodal load, it can be expressed as Eq. (3)

$$\mathbf{F}_{\text{ae}}^e = \mathbf{K}_{\text{ae}}^e\mathbf{X}^e + \mathbf{C}_{\text{ae}}^e\dot{\mathbf{X}}^e \tag{3}$$

where $\mathbf{F}_{\text{ae}}^e$ is the vector of the nodal aeroelastic forces. $\mathbf{K}_{\text{ae}}^e$ and $\mathbf{C}_{\text{ae}}^e$ represent the aeroelastic stiffness and damping matrices for element e, respectively, and can be expressed as Eq. (4). $\mathbf{X}^e$ and $\dot{\mathbf{X}}^e$ represent the nodal displacement and velocity vectors for element e, respectively, and can be expressed as Eq. (5)

$$\mathbf{K}_{\text{ae}}^e = \begin{bmatrix}\mathbf{K}_{\text{ae1}}^e & 0\\ 0 & \mathbf{K}_{\text{ae1}}^e\end{bmatrix}, \quad \text{where } \mathbf{K}_{\text{ae1}}^e = \frac{\rho U^2K^2l_e}{2}\begin{bmatrix}0&0&0&0&0&0\\0&H_4^*&0&BH_3^*&0&0\\0&0&0&0&0&0\\0&BA_4^*&0&B^2A_3^*&0&0\\0&0&0&0&0&0\\0&0&0&0&0&0\end{bmatrix} \tag{4a}$$

$$\mathbf{C}_{\text{ae}}^e = \begin{bmatrix}\mathbf{C}_{\text{ae1}}^e & 0\\ 0 & \mathbf{C}_{\text{ae1}}^e\end{bmatrix}, \quad \text{where } \mathbf{C}_{\text{ae1}}^e = \frac{\rho UBKl_e}{2}\begin{bmatrix}0&0&0&0&0&0\\0&H_1^*&0&BH_2^*&0&0\\0&0&0&0&0&0\\0&BA_1^*&0&B^2A_2^*&0&0\\0&0&0&0&0&0\\0&0&0&0&0&0\end{bmatrix} \tag{4b}$$

$$\mathbf{X}^e = [0 \;\; h_i \;\; 0 \;\; \alpha_i \;\; 0 \;\; 0 \;\; 0 \;\; h_j \;\; 0 \;\; \alpha_j \;\; 0 \;\; 0]^{\text{T}} \tag{5a}$$

$$\dot{\mathbf{X}}^e = [0 \;\; \dot{h}_i \;\; 0 \;\; \dot{\alpha}_i \;\; 0 \;\; 0 \;\; 0 \;\; \dot{h}_j \;\; 0 \;\; \dot{\alpha}_j \;\; 0 \;\; 0]^{\text{T}} \tag{5b}$$

where l_e is the length of element e, i and j the two nodes of bridge deck element e. The aeroelastic stiffness matrices $\mathbf{K}_{\text{ae}}^e$ and damping matrices $\mathbf{C}_{\text{ae}}^e$ are represented by

Matrix27 element in ANSYS and the global aeroelastic forces matrix $\mathbf{F}_{ae}$ can be expressed as Eq. (6)

$$\mathbf{F}_{ae}=\mathbf{K}_{ae}\mathbf{X}+\mathbf{C}_{ae}\dot{\mathbf{X}} \tag{6}$$

where $\mathbf{K}_{ae}$ and $\mathbf{C}_{ae}$ represent the global aeroelastic stiffness and damping matrices, respectively. Taking Eq. (6) into Eq. (1), the dynamic equations of a bridge can be expressed as Eq. (7)

$$\mathbf{M}\ddot{\mathbf{X}}+(\mathbf{C}-\mathbf{C}_{ae})\dot{\mathbf{X}}+(\mathbf{K}-\mathbf{K}_{ae})\mathbf{X}=\mathbf{0} \tag{7}$$

Flutter is a harmonic vibration and vibration equation can be assumed as $X=\phi e^{\lambda t}$, where $\lambda=\sigma\pm \mathrm{i}\omega$, real part of eigenvalue σ is the damping and imaginary part ω is the circular frequency of vibration. There is at least one damping larger than zero that the system is dynamic instability.

2.2 Identification of flutter derivatives

Numerical identification of flutter derivatives for cross-sections is a computational method based on CFD. In general, the aerodynamic forces acting on a plate can be expressed as Eq. (6)

$$L=\frac{1}{2}\rho U^2 BC_l, \qquad M=\frac{1}{2}\rho U^2 B^2 C_m \tag{6}$$

where C_i (i=l, m) are the dimensionless force coefficients. B represents the plate width.

In order to extract the flutter derivatives, a vertical or torsional harmonic vibration of circular frequency ω is imposed and the aerodynamic unsteady forces acting on the plate are recorded. After collecting enough data, the flutter derivatives are fitted out by Eq. (2). Application of dynamic mesh of CFD software FLUENT, the vibration of the cross-section is simulated through compiling the UDF code.

The cross-section of the plate is shown in Fig. 1. The computational conditions are given as follows: the ratio of width B to thickness H is 200 (B/H=200, and B=0.7m), and the amplitudes of harmonic vibration are $0.025B$ for vertical vibration and 3° for torsional vibration. The computational domain is assumed to be $24B$ long in the mean flow direction and $12B$ long in the cross-flow direction. Moreover, the section chord midpoint is assumed to be fixed for torsional vibration, and distant $6B$ from the velocity inlet boundary, and distant $18B$ from the pressure outlet boundary. In order to improve the calculation accuracy, the computational domain is divided into three regions, named as rigid mesh zone, dynamic mesh zone, and fixed mesh zone, respectively. The rigid mesh zone motions along with the plate to ensure the quality of the mesh near the plate. The rigid mesh zone and the fixed mesh zone have been discretized by a quadrilateral structured gird, and the dynamic mesh zone has been discretized by a triangular unstructured gird. The element size progressively increased from the side of plate to the computational boundary.

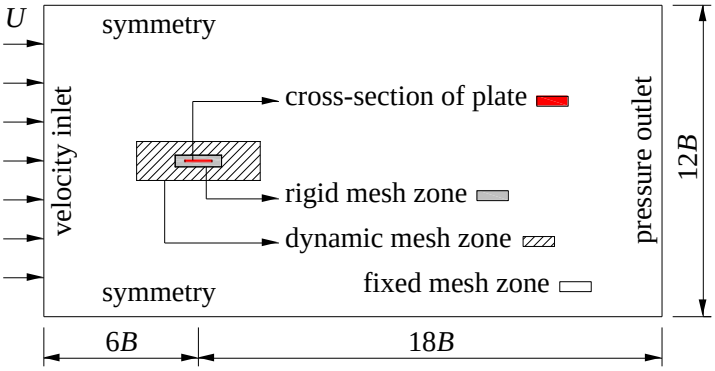

Fig. 1 Outline of the computational domain

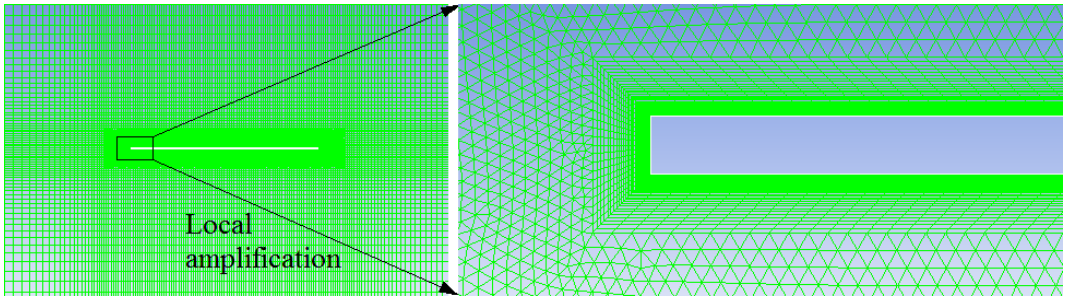

Fig. 2 Computational mesh employed for numerical analyses

The *k*-ω SST turbulence model is adopted and the dimensionless time-step has been set equal to 10^{-3}. The discretized problem has been numerically solved by adopting a SIMPLE pressure-velocity coupling algorithm. A second order scheme is selected for pressure, and a second order upwind scheme is selected for momentum, turbulent kinetic energy, and specific dissipation rate.

3. THE THIN FLAT PLATE

3.1 Theoretical flutter derivatives

In the classical theoretical case of steady sinusoidal oscillation of a 2-D ideal thin plate, using the Theodorsen's functions $F(K)$ and $G(K)$, the flutter derivatives can be expressed as Eq. (7)

$$H_1^* = -\frac{\pi}{K}F,\quad H_2^* = -\frac{\pi}{4K}\left(1+F+\frac{4G}{K}\right),\quad H_3^* = -\frac{\pi}{4K^2}(4F-KG),\quad H_4^* = \frac{\pi}{4K}(K+4G) \tag{7a}$$

$$A_1^* = \frac{\pi}{4K}F,\quad A_2^* = -\frac{\pi}{16K^2}(KF+4G-K),\quad A_3^* = \frac{\pi}{128K^2}(K^2+32F-8KG),\quad A_4^* = -\frac{\pi}{4K}G \tag{7b}$$

$$F(K) = 1-\frac{0.165}{1+\left(\frac{0.0455}{K/2}\right)^2}-\frac{0.335}{1+\left(\frac{0.3}{K/2}\right)^2},\quad G(K) = -\frac{\frac{0.165\times 0.0455}{K/2}}{1+\left(\frac{0.0455}{K/2}\right)^2}-\frac{\frac{0.335\times 0.3}{K/2}}{1+\left(\frac{0.3}{K/2}\right)^2} \tag{7c}$$

The constant term a of H_4^*, and b of A_3^* are not equal to zero, where a is equal to $\pi/4$, and b is equal to $\pi/128$. However, the flutter derivatives of bridge cross-sections have no theoretical solution, so it is not clear whether the constant term of flutter derivatives is equal to zero or not. Based on theoretical flutter derivatives of thin plate, the influence of constant term on calculation result is analyzed by ANSYS method as well as Scanlan's method. The parameters of the simply supported bridge model with ideal plate cross-section are given as follows:

span l=300m, width B=40m, vertical bending stiffness EI_z=2.1×10^{6}MPa·m^4,
lateral bending stiffness EI_y=1.8×10^{7}MPa·m^4, torsional stiffness GI_t=4.1×10^{5}MPa·m^4,
mass m=20000 kg/m, mass moment of inertia I_m=4500000kg·m^2/m,
air mass density ρ=1.225kg/m^3.

Keeping one constant term of H_4^* or A_3^* is invariant, the other one constant term is assumed to be –b/2, 0, b/2, b, 3b/2 (or –a/2, 0, a/2, a, 3a/2). The results of the flutter critical wind speed U_f are shown in Fig. 3. The flutter derivatives will change at all reduced wind velocity if the constant term is changed, so it will cause the value of U_f change. However, the change range of U_f is relatively small; for one reason, the influence of H_4^* on flutter performance for streamlined cross-section is relatively low (Zhang 2002) although the constant a is relatively large; for another reason, the influence of A_3^* on flutter performance for streamlined cross-section is relatively large, but the constant b is relatively small. The value of U_f is reduced when a is ignored, but increased when b is ignored. Therefore, the influence on flutter critical wind speed (U_f =136.2m/s) will become smaller if both a and b are not considered.

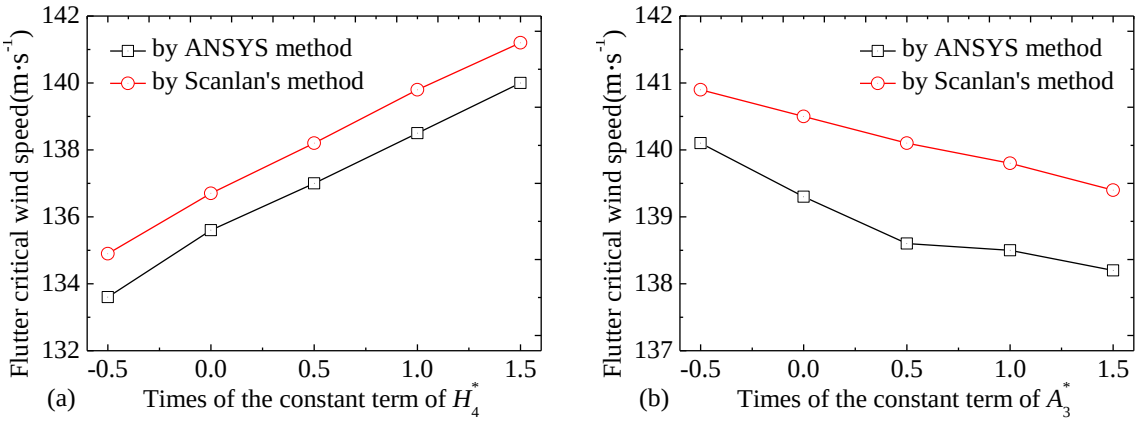

Fig. 3 Flutter critical wind speeds under different constant terms

In most cases, the value of constant term is not known. Generally, the flutter derivatives are assumed to be zero when wind velocity is equal to zero. For this case, theoretical H_4^* and A_3^* with a finite number at different reduced wind velocity (V=2, 4, 6,

8, 10, 12, 14) are selected and assumed to be zero for V=0. By these data mentioned above, fitting a curve and calculating the flutter critical wind speed. The results (U_f =138.5m/s by ANSYS method, U_f =139.6m/s by Scanlan's method) are very closed to the theoretical solution (in Fig.3). The main reason is the flutter derivatives change at low reduced wind velocity only, but unchanged at high reduced wind velocity. The flutter derivatives obtained from wind tunnel test or numerical simulation have contained constant term. Therefore, assuming the flutter derivatives to be zero when wind velocity is equal to zero is reasonable.

3.2 Aerodynamic coefficients

The equations of aerodynamic coefficients can be expressed as Eq. (8)

$$C_l = 2\pi\alpha, \quad C_m = C_l / 4 \tag{8}$$

where α is the wind attack angle.

Based on the flat plate, the aerodynamic performance is calculated by CFD software FLUENT to check the rationality of the mesh generation. The values of calculation parameters and mesh generation have been introduced. Lift coefficient and moment coefficient of the plate about the mid-chord are shown in Fig. 4. Streamline diagrams of mean velocity vector at some wind attack angles are shown in Fig. 5.

In the low-angle region (α≤4°), results are consistent with the thin airfoil theory. The plate presents the characteristic of streamlined cross-section (Fig. 5a and 5b). The lift coefficient is about four times as big as moment coefficient. The slope of the lift curve becomes smaller and the value of the moment coefficient begins to decrease for α>6°, and the plate begins to present the characteristic of bluff body (Fig. 5c). The trends of the coefficients are similar with Amandolese (2013). According to Fig. 5, the length of a leading-edge laminar separation bubble from the leading edge to the reattachment point increases gradually with the wind attack angle. The upstream separated airflow cannot reattach to the plate for α>6°, and the aerodynamic coefficients are no longer equal to the thin airfoil theory.

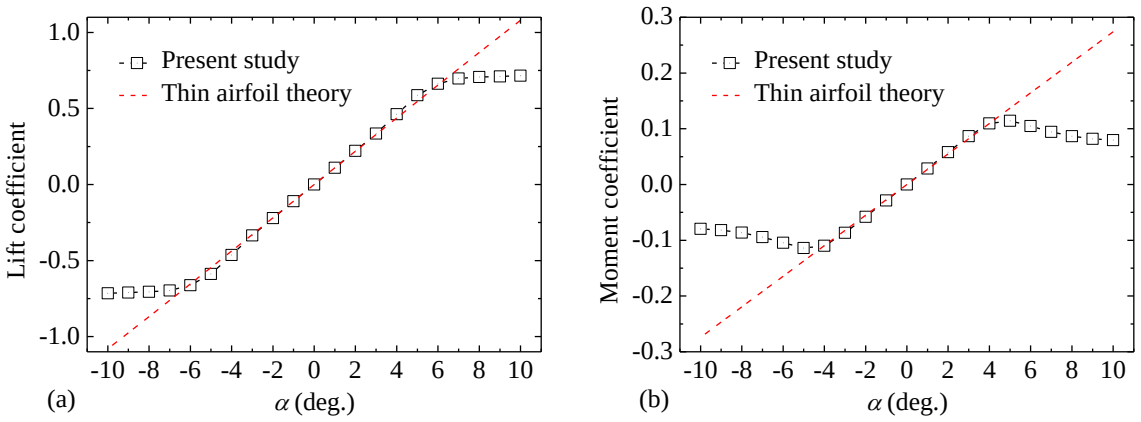

Fig.4 Lift coefficients and moment coefficients under different wind attack angles

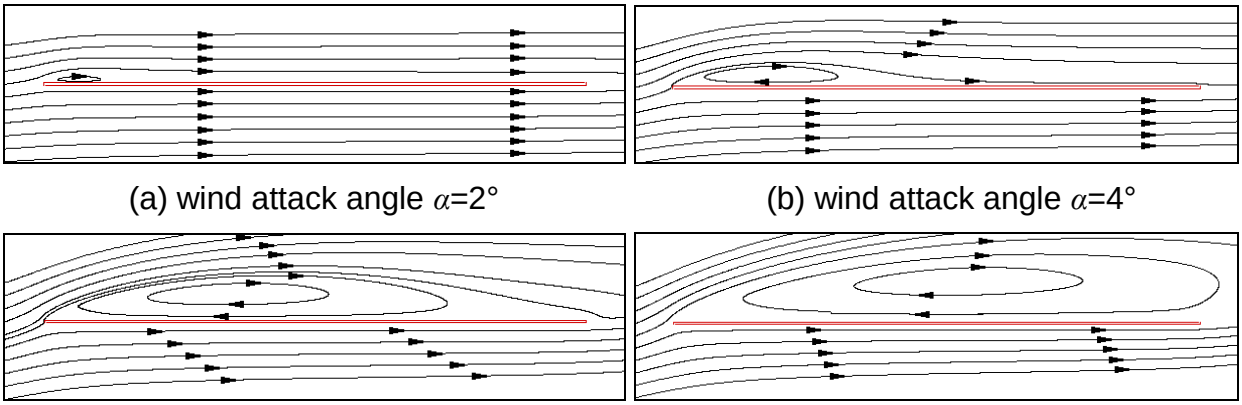

(a) wind attack angle α=2° (b) wind attack angle α=4°

(c) wind attack angle α=6° (d) wind attack angle α=8°

Fig.5 Streamline diagrams of mean velocity vector

3.3 Numerical results of flutter derivatives

The flutter derivatives of flat plate are calculated for α=0° to check the reliability of the analysis method. The simulations cover the reduced wind velocity range from 2 to 14. The computed aerodynamic derivatives are compared with Theodorsen's theoretical solutions. As shown in Fig. 6, all simulated aerodynamic derivatives are in quite good agreement with theoretical solutions.

According to the analysis method mentioned above, all flutter derivatives are assumed to be zero when reduced wind speed is equal to zero. Fitting a curve and calculating the flutter critical wind speed U_f, the results are shown in Table. 1. The U_f calculated by numerical solution agrees with the result calculated by theoretical solution (in Fig.3). The difference between the two results is mainly caused by the difference between the theoretical and numerical flutter derivatives at high reduced wind speed.

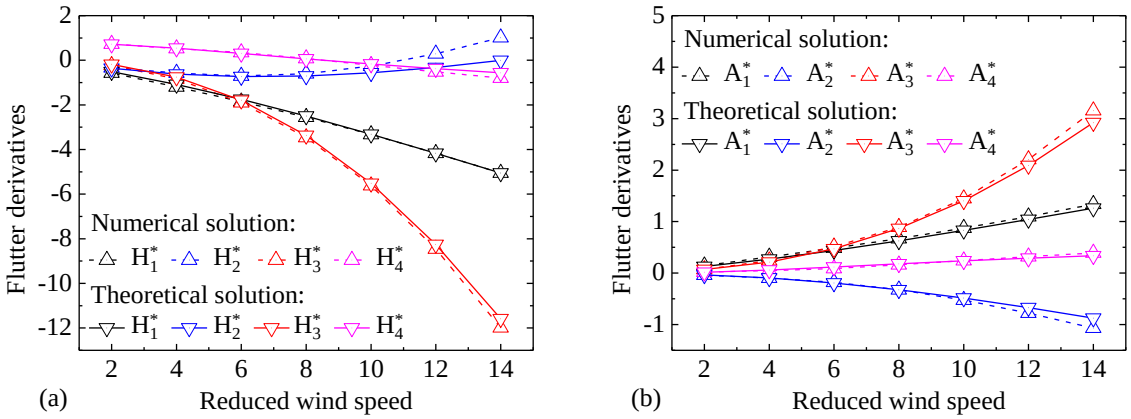

Fig. 6 Flutter derivatives of theoretical and numerical solution

Table 1 Flutter critical wind speed by different analysis method

Analysis method	ANSYS method	Scanlan's method
U_f by theoretical flutter derivatives	138.5 m/s	139.8 m/s
U_f by numerical flutter derivatives	136.2 m/s	137.5 m/s

4. FLUTTER PERFORMANCE OF CENTRAL-SLOTTED PLATE

Flutter performance of a bridge deck will change significantly with the increase of wind attack angle. In complicated mountain area, large wind attack angle is a common situation. It is important to analysis what change of flutter performance will occur and how to improve the flutter critical wind speed under large wind attack angles. Central-slotted deck is a typical optimization measure for long-span bridges. The effects on the flutter performance of central-slotted plate are discussed under the condition of various slot widths and wind attack angles. The central-slotted plate is shown in Fig. 7. The computational conditions of central slotted plate are the same as the plate's mentioned above. Keeping the B=0.7m, the slot ratio D/B ranges from 0.05 to 0.20 by increasing the slot width D, and the wind attack angle α ranges from 0 degrees to 6 degrees.

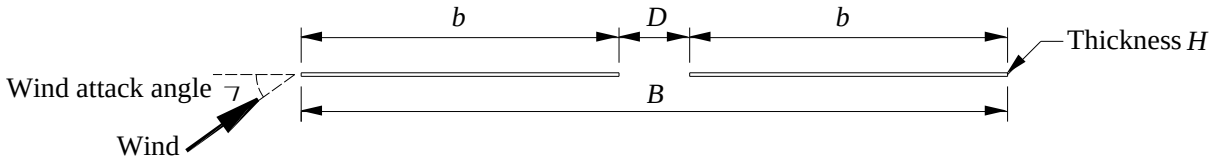

Fig. 7 Cross-section of the central-slotted plate

4.1 Flutter critical wind speeds

The flutter derivatives of plate for each wind attack angle and slot ratio using the CFD method are computed. The flutter critical wind speeds of the simply supported bridge model mentioned above are then calculated and shown in Fig. 8. Partial flutter derivatives are shown in Fig. 9. No matter whether the plate is slotted or not and what the slot ratio is, the flutter critical wind speed decreases with the increase of wind attack angle. Therefore, the wind attack angle is a negative factor for the flutter performance.

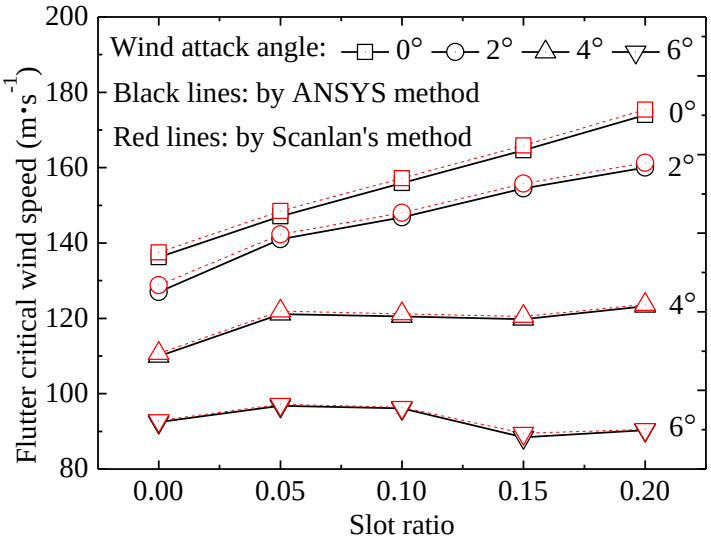

Fig. 8 Flutter critical wind speed of the central-slotted plate

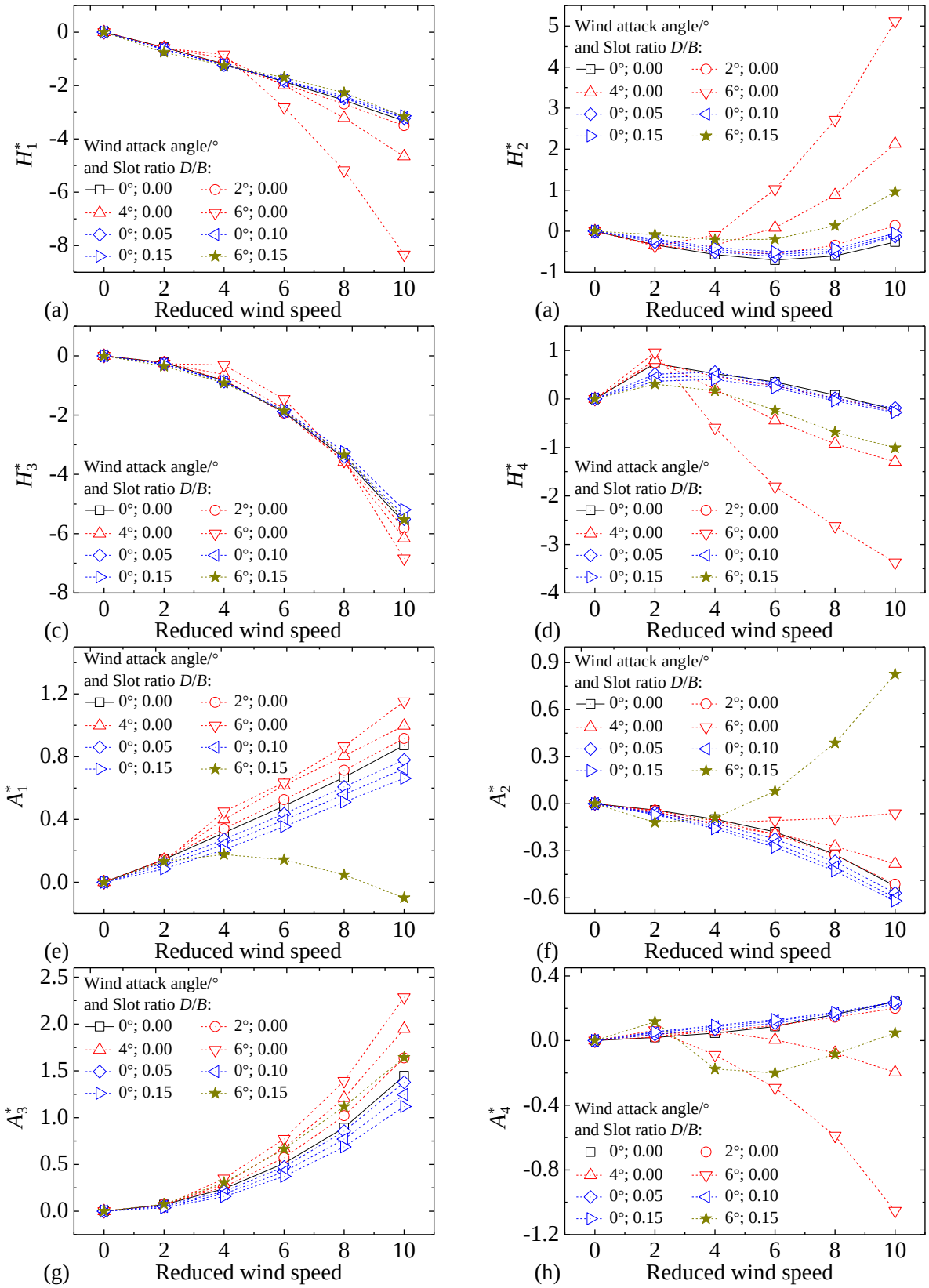

Fig. 9 Flutter derivatives of the central-slotted plate

When the wind attack angle is equal to 0 or 2 degrees, the plate is similar with streamlined cross-section, and the critical wind speed increases with the increase of slot ratio. When the wind attack angle is equal to 4 degrees, though slotting can improve the critical wind speed, the effect is limited that critical wind speeds are similar with each other under different slot ratios (range from 0.05 to 0.20). However, when the wind attack angle is equal to 6 degrees, the plate presents the characteristic of bluff body, and its critical wind speed for D/B=0.15 or 0.20 is smaller than D/B=0. In other words, the central-slotting can improve the critical wind speed of plate for low wind attack angle, but it will become a negative factor when the wind attack angle is large enough to make a streamlined cross-section present the characteristic of bluff body.

4.2 Flutter performance of plate under different wind attack angles

The flutter critical wind speed decreases with the increase of wind attack angle for all slot ratios. Take the plate with D/B=0 for example, its flutter derivatives are shown in Fig. 9. The wind attack angle has significant influence on the flutter derivatives especially A_2^* and A_4^* which are related to torsion movement. The instantaneous streamline and static pressure diagrams of t=1/4T, 1/2T, 3/4T are shown in Fig. 10 for torsional harmonic vibration and Fig. 11 for vertical harmonic vibration, where T is the vibration period. When the wind attack angle is 0, 2 or 4 degrees, the value of A_2^* decreases with the increase of reduced wind speed and is always less than zero. The plate presents the characteristic of streamlined body with uniform distribution of static pressure, and the vortex only exists in front of the plate. For streamlined section, bending and torsion movement have strong coupling effect, so the coupled bending-torsional flutter of plate will occur at the critical wind speed. However, the vortex and the area of negative pressure above the plate increase with the increase of wind attack angle, so the plate gradually presents the characteristic of bluff body. When the wind attack angle is equal to 6 degrees, different trend of A_2^* occurs, so the coupled bending-torsional flutter of plate will converted to torsional flutter that can decreases the flutter critical wind speed.

Modal analysis of the simply supported bridge model mentioned above without aeroelastic stiffness and damping matrices, was conducted by ANSYS method. The first 7 natural frequencies and vibration modes are shown in Table 2. Modals (1, 4, 7) are related to vertical vibration, and modals (2, 5, 6) are related to torsional vibration. The bridge model with aeroelastic forces matrix was then calculated, and complex eigenvalues under different wind velocities and wind attack angles (α=0°, 2°, and 6°, for example) are shown in Fig. 12. For vertical modal 1, 4, or 7, the damping decreases with the increase of wind speed. For torsional modal 2, 5, or 6, the damping decreases first with the increase of wind speed, and then it appears to be an increase trend. The lower the order number is, the easier the increase trend appears, so the modal 2 is a key factor in flutter. When the damping of modal 2 is close to zero, the flutter will occur. With the increase of wind attack angle, the increase trend of torsional modal appears at lower wind speed. Therefore, the critical wind speed is decreases with the increase of wind attack angle.

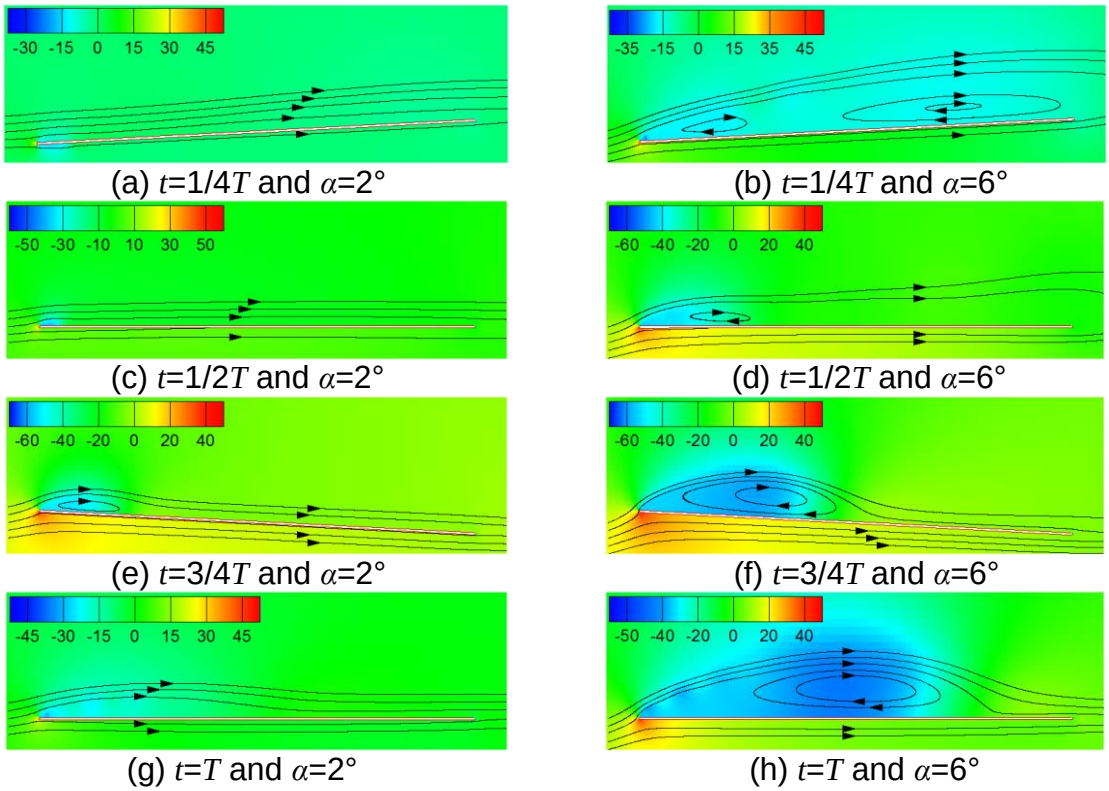

(a) t=1/4T and α=2° (b) t=1/4T and α=6°

(c) t=1/2T and α=2° (d) t=1/2T and α=6°

(e) t=3/4T and α=2° (f) t=3/4T and α=6°

(g) t=T and α=2° (h) t=T and α=6°

Fig. 10 Instantaneous streamline and static pressure for torsional vibration (D/B=0)

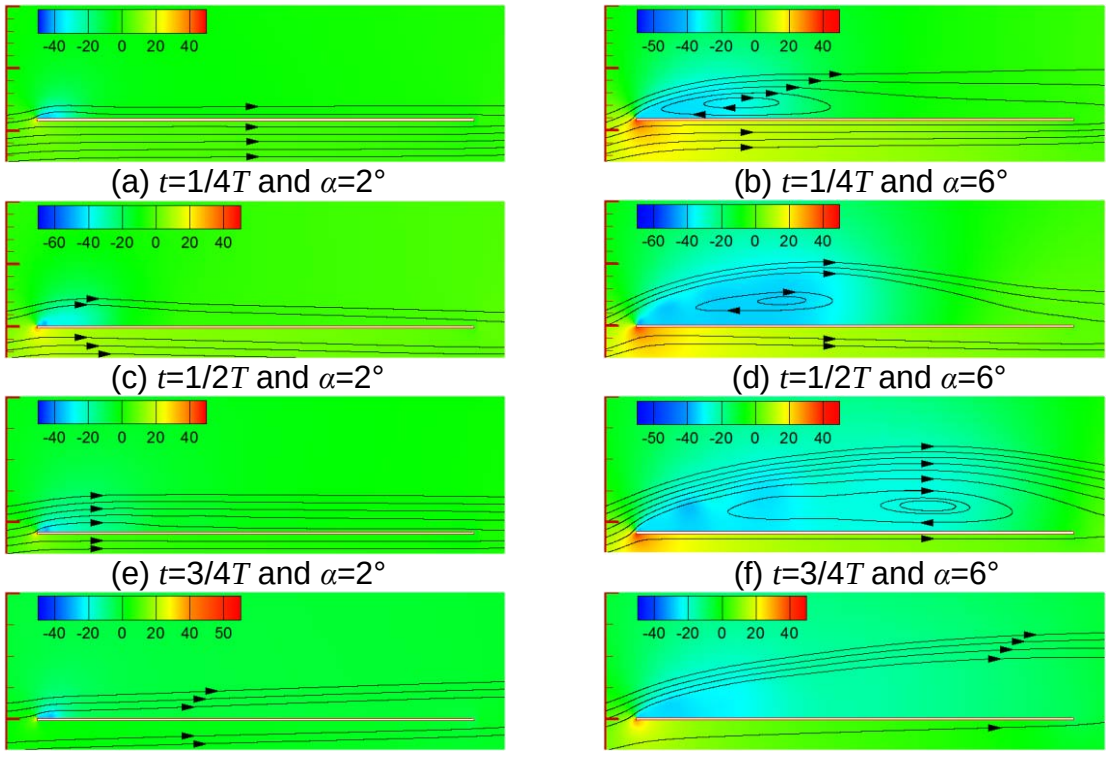

(a) t=1/4T and α=2° (b) t=1/4T and α=6°

(c) t=1/2T and α=2° (d) t=1/2T and α=6°

(e) t=3/4T and α=2° (f) t=3/4T and α=6°

(g) t=T and α=2° (h) t=T and α=6°

Fig. 11 Instantaneous streamline and static pressure for vertical vibration (D/B=0)

Table 2
Vibration modes and frequencies of bridge model without aeroelastic forces matrix

Order number	1	2	3	4	5	6	7
Frequency(Hz)	0.179	0.503	0.524	0.715	1.004	1.503	1.610
Vibration moad	S-V	S-T	S-L	AS-V	AS-T	S-T	S-V

Note: S – symmetric; AS – antisymmetric; L – lateral; V – vertical; T – torsional.

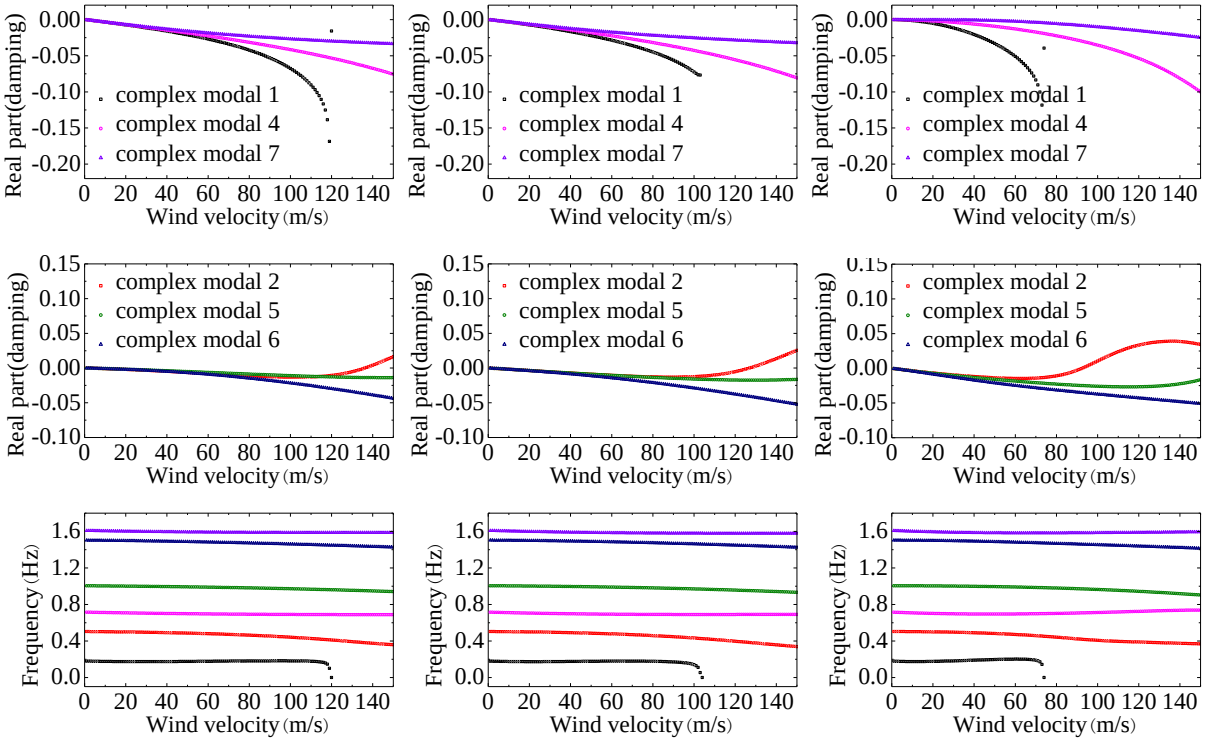

(a) α=0° (b)α=2° (c)α=6°

Fig. 12 Complex eigenvalues of model under different wind attack angles (D/B=0)

4.3 Flutter performance of plate under different slot ratios

Take the plate with D/B=0.15 for example, the instantaneous streamline and static pressure diagrams of t=1/4T, 1/2T, 3/4T are shown in Fig. 13 for torsional harmonic vibration and Fig. 14 for vertical harmonic vibration.

When the wind attack angle is equal to 0 degrees, Fig. 9 shows that all the derivatives of plate under different slot ratios have the same trend. Compared with the plate for D/B=0, slotting does not change the trend of flutter derivatives. The central-slotted plate can be divided into two independent plates. For upstream side, there is no significant change of the static pressure and the streamline between the plate (D/B=0) and the central-slotted plate (D/B=0.15) according to Fig. 10, 11, 13, 14. However, a similar negative pressure region form in front of downstream side, but its area and value are smaller than the upstream negative pressure region due to the aerodynamic disturbance. The existence of the downstream negative pressure region can offset the effect of the upstream negative pressure region. For the whole plate, its stability will inc-

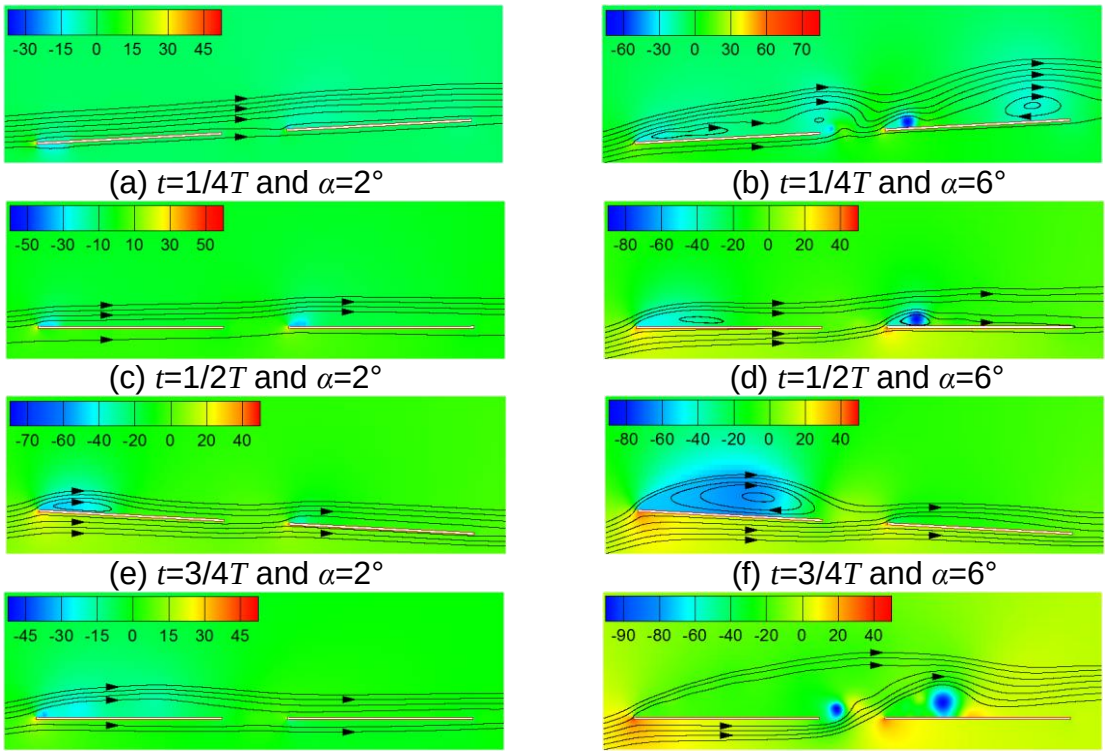

(a) t=1/4T and α=2° (b) t=1/4T and α=6°

(c) t=1/2T and α=2° (d) t=1/2T and α=6°

(e) t=3/4T and α=2° (f) t=3/4T and α=6°

(g) t=T and α=2° (h) t=T and α=6°

Fig. 13 Instantaneous streamline and static pressure for torsional vibration (D/B=0.15)

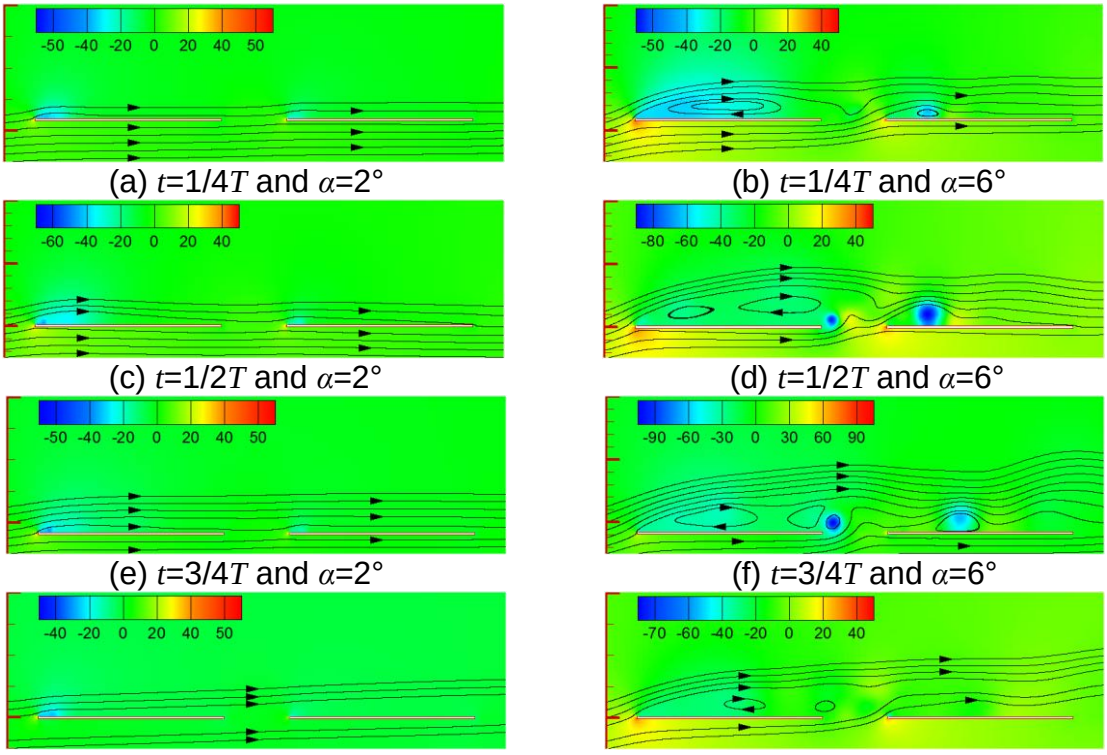

(a) t=1/4T and α=2° (b) t=1/4T and α=6°

(c) t=1/2T and α=2° (d) t=1/2T and α=6°

(e) t=3/4T and α=2° (f) t=3/4T and α=6°

(g) t=T and α=2° (h) t=T and α=6°

Fig. 14 Instantaneous streamline and static pressure for vertical vibration (D/B=0.15)

rease. With the increase of D/B, the aerodynamic disturbance is gradually weakened and the negative pressure region of the downstream side is more close to the upstream side. For the whole plate, the effect of the upstream negative pressure region is further weakened, so its flutter stability will increase.

When the wind attack angle is equal to 6 degrees, central-slotting makes the flow field more turbulent, and the absolute value of negative pressure increased obviously. Compared with the plate with no slotting for α=6°, A_1^* and A_2^* have significant change when D/B is equal to 0.15. Although the changes of H_1^*, H_2^*, H_3^*, H_4^*, A_3^*, A_4^* are favorable for flutter stability, the flutter critical wind speed will still decrease due to the advance of the value of A_2^* become positive.

Complex eigenvalues of the plate for D/B=0.15 under different wind attack angles (α=0°, 2°, and 6°, for example) are shown in Fig. 14. For torsional modal 2, 5, or 6, large wind attack angle has greater effect on damping than frequency, because A_1^* and A_2^* are elements of the damping matrix $\mathbf{C}_{ae}^e$ (Eq. 4). Compared with the plate without slotting, slotting can decrease the damping of torsional modal for α=0° or α=2°, so the flutter critical wind speed increases. For α=6°, instead of decreasing the damping of modal 2, slotting make its value to zero earlier, so the flutter critical wind speed decreases.

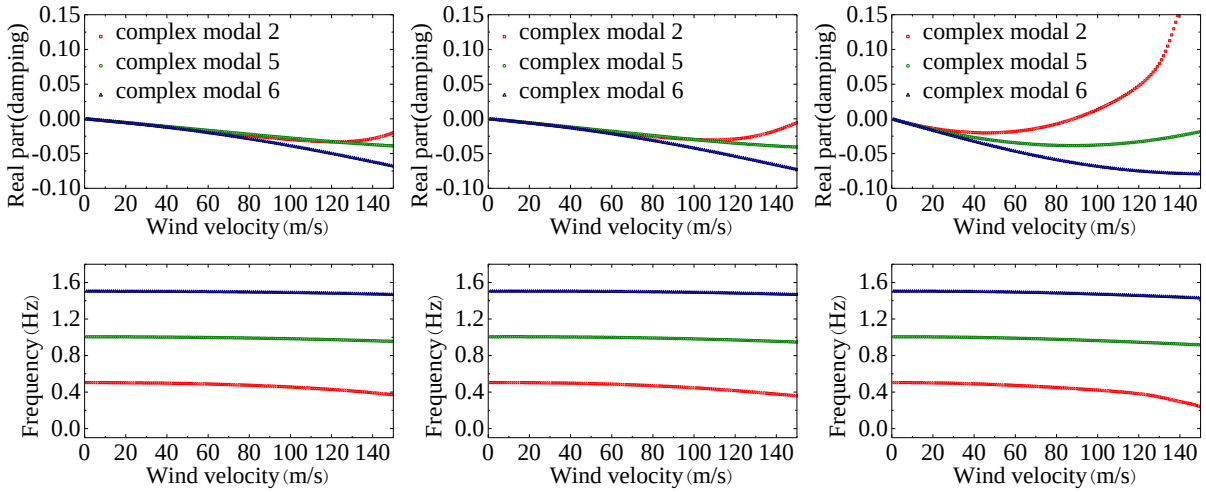

(a) α=0° (b)α=2° (c)α=6°

Fig. 15 Complex eigenvalues of model under different wind attack angles (D/B=0.15)

5. CONCLUSIONS

In this study, the ANSYS software and CFD software FLUENT are employed to perform flutter analysis on the plate and central-slotted plate. The influences of slot widths and wind attack angles on the flutter stability of a bridge model are investigated and the following conclusions are made:

(1) Assuming the flutter derivatives to be zero when wind velocity is equal to zero is reasonable, because it has little effect on flutter derivatives at high reduced wind velocity and the flutter derivatives obtained from wind tunnel test or numerical simulation have contained constant term.
(2) The plate presents the characteristic of streamlined body for $\alpha \leq 4°$, the aerodynamic coefficients are consistent with the thin airfoil theory and the lift coefficient is about four times as big as moment coefficient. The slope of the lift curve becomes smaller and the value of the moment coefficient begins to decrease for $\alpha > 6°$ and the plate begin to present the characteristic of bluff body due to the upstream separated airflow cannot reattach to the plate.
(3) No matter whether the plate is slotted or not and what the slot ratio is, the flutter critical wind speed decreases with the increase of wind attack angle. When the attack angle is 6 degrees, the coupled bending-torsional flutter of plate will converted to torsional flutter that can decreases the flutter critical wind speed.
(4) When the wind attack angle is small (α=0°, 2°), slotting is an effective measure to improve the flutter stability of plate. When the wind attack angle is equal to 4 degrees, the effect of slotting on flutter stability is limited. When the wind attack angle is large enough (α=6°) to make the plate present the characteristic of bluff body, slotting will become a negative factor for the flutter stability.

ACKNOWLEDGMENTS

The supports from the National Natural Science Foundation of China (No. 51278434), the National Key Technology R&D Program (No. 2012BAG05B02) are greatly acknowledged.

REFERENCES

Scanlan, R.H. (1978), “The action of flexible bridges under wind, I: flutter theory,” *J. Sound Vib.,* **60**(2), 187-199.
Namini, A., Albrecht, P. (1992), “Finite element-based flutter analysis of cable-suspended bridges,” *J. Struct. Eng., ASCE,* **118**(6), 1509-1526.
Chen, Z.Q. (1994), “The three dimensional analysis and behaviors investigation on the critical flutter state of bridges,” *Proceedings of the Symposium on cable-stayed bridges, Shanghai, China*.
Ding, Q.S., Chen, A.R., Xiang, H.F. (2002), “Coupled flutter analysis of long-span bridges by multimode and full-order approached,” *J. Wind Eng. Ind. Aerodyn.,* **90**(12-15), 1981-1993.
Miyata, T., Yamada, H. (1990), “Coupled flutter estimate of a suspension bridge,” *J. Wind Eng. Ind. Aerodyn.,* **33**(1-2), 341-348.
Ge, Y.J., Tanaka, H. (2000), “Aerodynamic flutter analysis of cable-supported bridges by multi-mode and full-mode approaches,” *J. Wind Eng. Ind. Aerodyn.,* **86**(2-3), 123-153.
Steinman, D.B. (1956), “The design of the Mackinac Bridge for aerodynamic stability,” *Journal of the Franklin Institute.,* **262**(6), 453-468.
Miyata, T., Yamaguchi, K. (1993), “Aerodynamics of wind effects on the Akashi Kaikyo Bridge,” *J. Wind Eng. Ind. Aerodyn.,* **48**(2-3), 287-315.

Sato, H., Hirahara, N., Fumoto, K., Hirano, S. and Kusuhara, S. (2002), "Full aeroelastic model test of a super long-span bridge with slotted box girder", *Journal of Wind Engineering and Industrial Aerodynamics,* **90**(12-15), 2023-2032.

Scanlan, R.H. (1993), "Problematic in formulation of wind-force model for bridge decks," *J. Struct. Eng., ASCE,* **119**(7), 1433-1446.

Zhang, X.J., Chen, A.R., Xiang, H.F., Peng, W. (1956), "Study of flutter mechanism of long-span bridges with different main girder sections," *China Journal of Highway and Transport.,* **15**(2), 52-56. (in chinese)

Amandolese, X., Michelin, S. and Choquel, M. (2013), "Low speed flutter and limit cycle oscillations of a two-degree-of-freedom flat plate in a wind tunnel", *Journal of Fluids and Structures,* **43**(8), 244-255.